HHS Public Access

Author manuscript

Nat Immunol. Author manuscript; available in PMC 2012 November 01.

Published in final edited form as:

Nat Immunol. ; 13(5): 499–510. doi:10.1038/ni.2262.

Transcriptional profiling of stroma from inflamed and resting lymph nodes defines immunological hallmarks

Deepali Malhotra[1,2,‡], **Anne L. Fletcher**[1,‡], **Jillian Astarita**[1,2], **Veronika Lukacs-Kornek**[1], **Prakriti Tayalia**[3], **Santiago F. Gonzalez**[4], **Kutlu G. Elpek**[1], **Sook Kyung Chang**[5], **Konstantin Knoblich**[1], **Martin E. Hemler**[1,5], **Michael Brenner**[5,6], **Michael C. Carroll**[4], **David J. Mooney**[3], **Shannon J. Turley**[1,7], and **Immunological Genome Project Consortium**

[1]Department of Cancer Immunology and AIDS, Dana Farber Cancer Institute, Boston, MA 02115, USA

[2]Division of Medical Sciences, Harvard Medical School, Boston, MA 02115, USA

[3]School of Engineering and Applied Sciences, Harvard University, Cambridge, MA 02138, USA

[4]The Immune Disease Institute and Program in Cellular and Molecular Medicine, Children's Hospital, Department of Pediatrics and Department of Pathology, Harvard Medical School, Boston, MA, USA

[5]Brigham and Women's Hospital, Boston MA 02115, USA

[6]Department of Medicine, Division of Rheumatology, Immunology and Allergy, Harvard Medical School, Boston, MA 02115, USA

[7]Department of Microbiology and Immunobiology, Harvard Medical School, Boston, MA 02115, USA

Abstract

Lymph node stromal cells (LNSCs) closely regulate immunity and self-tolerance, yet key aspects of their biology remain poorly illuminated. Comparative transcriptomic analyses of murine LNSC subsets revealed expression of important immune mediators, growth factors, and novel structural components. Pairwise analyses of ligands and cognate receptors across hematopoietic and stromal subsets suggested a complex web of cross-talk. Compared with skin and thymic fibroblasts, fibroblastic reticular cells (FRCs) were enriched in genes relevant to cytokine signaling. LNSCs from inflamed lymph nodes upregulated acute phase response genes, chemokines, and antigen presentation genes. Poorly studied podoplanin^{-}CD31^{-} LNSCs showed similarities to FRCs, but

Correspondence: Shannon J. Turley shannon_turley@dfci.harvard.edu Tel: 617.632.4990 Fax: 617.582.7999.

‡These authors contributed equally to this work.

Database accession number All ImmGen raw data (stromal and hematopoietic) are available from the NCBI GEO database (GSE 15907), and can be queried in processed form on the project's data browsers (www.immgen.org).

Author contributions D.M. and A.L.F. designed the study, performed and analyzed most experiments, and wrote the manuscript. S.J.T. directed the study, analyzed and interpreted results, and co-wrote the manuscript. D.M. performed primary analysis of the microarray data. V.L.K., P.T., S.F.G., J.A., K.G.E., and K.K. performed and analyzed individual experiments. S.K.C., M.B., D.J.M., M.C.C., and M.E.H. contributed reagents and assisted with analysis of individual experiments.

lacked IL-7 expression, and were identified as myofibroblastic integrin $\alpha 7^+$ pericytes. Together these data comprehensively describe the transcriptional characteristics of LNSC subsets.

INTRODUCTION

The Immunological Genome Project (ImmGen) is a multi-center collaborative venture involving immunologists and computational biologists aiming to build a comprehensive, publicly accessible database of gene expression and regulatory networks in the immune system of the mouse. Data generation involves shared, rigorously controlled methodology and analysis pipelines[1]. As part of this collaboration, we meticulously analyzed the transcriptomes of lymph node stromal cells (LNSCs) under steady-state and inflammatory conditions.

LNSCs are non-hematopoietic cells crucial for the normal functioning of the immune system, yet they are difficult to study and comprise ~1% of LN cellularity. Podoplanin (gp38) and platelet endothelial cell adhesion molecule 1 (CD31) expression distinguish LNSC subsets: $gp38^+CD31^-$ fibroblastic reticular cells (FRCs), $gp38^+CD31^+$ lymphatic endothelial cells (LECs), $gp38^-CD31^+$ blood endothelial cells (BECs), and $gp38^-CD31^-$ double negative cells (DNCs)[2]. LNSCs play distinct roles in orchestrating immune responses, while FRCs and LECs also promote tolerance[3-7]. LECs facilitate the entry of antigen-bearing dendritic cells (DCs) and soluble antigens into LNs[3], and control lymphocyte egress[8], while BECs form vessels that allow naive lymphocytes to enter LNs through high endothelial venules (HEVs)[3]. Inside the LN, FRCs construct and regulate a specialized reticular network of fibers used by lymphocytes and DCs as a scaffold on which to migrate and interact[3]. Ensheathed by FRCs, the reticular network also forms a complex conduit system of microchannels that rapidly conduct chemokines and other small factors (<70kDa) from the subcapsular sinus to HEVs[9,10]. During infection, chemokine decoration of HEVs attracts leukocytes to LNs, promoting the adaptive immune response[11]. FRCs also secrete survival factors and chemokines that attract T cells and DCs[2,3]. Indeed, DCs contacting the reticular network can process tissue-derived soluble antigens, suggesting that conduit-borne lymph may be an important source of antigens during early phases of immune responses or for the maintenance of peripheral tolerance[9,12].

Despite maintaining naive lymphocytes, regulating immune responses, and orchestrating DC-T cell interactions, relatively little is known about how FRCs, LECs, and BECs interact and are regulated in post-natal life. Moreover, FRC-like cells identified in autoinflammatory or cancerous lesions are associated with worsened clinical outcomes[13,14]. Nonetheless, our knowledge of the transcriptional identity of FRCs is limited, essentially consisting of a generic myofibroblastic phenotype expressing identified specialized elements such as chemokines. Recent evidence suggests that FRCs and LECs may also play important roles in tolerance induction, yet expression of pathogen receptors and antigen-presenting machinery is almost completely unstudied.

Transcriptomics is a powerful, unbiased starting point for uncovering a cell's biology, identifying large numbers of new targets for further study, including molecular pathways, surface receptors, and secreted factors. To date, transcriptomics has not been used to

examine the specialization of multiple stromal cell types. We therefore aimed to create a comprehensive, cross-comparable database of stromal transcriptional profiles.

We analyzed the transcriptomes of FRCs, LECs, BECs, and poorly-studied DNCs[2,6,7], identifying and analyzing each subset's unique expression signature. We matched expression of immune mediators and growth factors to cognate receptors on likely hematopoietic and stromal partners. Analysis of steady-state LNSCs also suggested a readiness to respond to inflammatory or infectious triggers, a hypothesis further explored by profiling of LNSCs that we isolated during an immune response. Next, we more fully characterized the molecular makeup of the LN reticular network. We observed substantial differences in the transcriptional profiles of FRCs and their skin and thymic counterparts, reflecting functional specialization. Finally, while the lineage, function, localization, and identifying surface markers of DNCs were all previously unknown[2,6,7], this in-depth analysis showed that this subset consisted largely of contractile, FRC-like pericytes.

RESULTS

Comparative transcriptional distances between LNSC subsets

To obtain transcriptomes for each subset, FRCs, LECs, BECs, and DNCs were sorted to high purity from stromal-enriched fractions of LNs from 10-30 C57BL/6 mice per replicate (Fig. 1a,b and Supplementary Fig. 1a,b). Using the ImmGen profiling and quality control (QC) pipelines[1], gene expression profiles were generated on Affymetrix MoGene 1.0 ST arrays. All data analyzed below passed ImmGen QC, with good replicate quality (median inter-replicate coefficients of variation (CVs) of 0.086-0.205). The general ImmGen post-normalizaton threshold of 120 was taken to indicate positive expression (at 95% confidence), and probes were included in comparisons only if they were expressed by at least one cell type and showed low variability within populations (see On-line methods). Inspection of the data demonstrated expression of the expected markers, and samples were negative for common hematopoietic markers (Fig. 1c and Supplementary Fig. 1c,d).

Global relationships among sorted LNSCs were examined using principal component analysis (PCA), based on the 15% most differentially expressed probes. This mathematical transformation reduces multi-dimensional expression data into principal components (PCs), each of which accounts for a proportion of total variability (Fig. 1d). Within each cell type, skin-draining and mesenteric LN (SLN, MLN) samples clustered tightly, reflecting conservation of subset-specific genes between these tissues. Along the first two PCs, accounting for 83.5% of observed variability, FRCs and DNCs were positioned closer to each other than either endothelial subset. However, FRCs and DNCs clearly separated along the third PC, demonstrating a transcriptionally distinct relationship. These relationships were also evident on matrix plots of population concordance (measured by Pearson's correlation and Euclidean distance) (Fig. 1e and Supplementary Fig. 1e). Hierarchical clustering of differentially expressed probes reinforced relative transcriptional similarities between FRCs and DNCs, and LECs and BECs (Fig. 1f)[15]. These data show that stromal subsets from different locations do not undergo marked site-specific differentiation, and that DNCs share more transcriptional similarity with FRCs than with LECs or BECs.

Identifying LNSC subset-specific genes and pathways

Next, FRCs were compared with BECs and LECs to identify subset-specific transcriptional signatures (Fig. 2a). A count of probes showing a differential expression >2 was used as a simple metric of transcriptional differences; SLN FRCs differed from SLN BECs and LECs by 2,026 and 1,936 probes respectively (Fig. 2a). These differences were highly conserved in SLNs and MLNs, evidenced by the distribution of probes along the diagonal in the FoldChange/FoldChange plot.

Probes upregulated in SLN FRCs relative to one endothelial cell (EC) subset, also tended to be upregulated relative to the other EC subset (>91.3% of probes; chi-square test $P<0.0001$; Fig. 2b), highlighting the closer developmental relationship between LECs and BECs. In fact, SLN BECs and LECs differed in expression of fewer probes **(**Fig. 2c**)**, and on average these differences were of a smaller magnitude than between ECs and FRCs. This pattern was also highly conserved in the MLN **(**Fig. 2c**)**.

To better understand how FRCs differed from sorted ECs, we identified 594 FRC-specific and 513 EC-specific (upregulated in LECs and BECs) probes (delta score (δ)=1.0 (adjusted fold change (FC)≥2) for at least one comparison and δ=0.85 (adjusted FC≥1.8) for all other comparisons; $P<0.05$ for differences in EV) (Supplementary Tables 1 and 2). The delta score module computes adjusted FCs between two populations, minimizing noise by exponentially penalizing FCs for intrapopulation variability.

To identify novel, immunologically relevant genes and pathways associated with these cells, signature probe lists were analyzed by collating genes into functional pathways of the KEGG database and ranking these pathways based on statistical overrepresentation using DAVID[16]. FRC-specific probes were enriched for extracellular matrix (ECM)-receptor interactions, focal adhesion, and cytokine-cytokine receptor interactions (Fig. 2d). In contrast, EC-specific probes were enriched for genes relevant to leukocyte transmigration. EC-specific probes also showed enrichment for VEGF signaling and cell-cell adhesion (Fig. 2d), vital for regulating vessel integrity and permeability. These global overviews confirmed known stromal functions, allowing us to simultaneously comb cell-specific lists for genes not previously reported in LNSCs, while providing clues to their likely function.

Molecular communication within the LN

FRC enrichment in cytokine-related genes was explored by examining LNSC expression of cytokines, growth factors and immunologically relevant receptors, paired with expression of cognate ligands and receptors by stroma and key hematopoietic populations (Fig. 3a,b). LNSCs were identified as rich sources of signals and growth factors recognized by hematopoietic cells (Fig. 3a,b). LNSCs shared expression of receptors for common immune mediators such as type I and type II interferons, TGF-β, and TNF, however, subsets also exhibited unique transcriptional profiles for cytokine and chemokine responsiveness, pathogen recognition, and costimulatory potential (Fig. 3a,b and Supplementary Fig. 2a,b).

Interleukin (IL)-7 crucially maintains naive lymphocytes within LNs[2,3], and while IL-7 mRNA has been observed in FRCs,10-fold lower transcript levels in pooled ECs have also been detected[2]. We found that FRCs and LECs produced lL-7 transcript while BECs and

DNCs did not (Fig. 3a). Further, T cells, natural killer (NK) cells, NKTs, and DCs expressed IL-7Rα chain mRNA (Fig. 3a). FRCs expressed the B cell survival factor and T cell costimulator[17] BAFF. FRCs also produced transcripts for molecules that support myeloid cells, including IL-34, which binds macrophage colony stimulating factor 1 receptor[18]; Flt3L, shown to bind Flt3 and support DC development, maintenance, and expansion[19]; and the monocyte-DC chemoattractant CXCL14 (Fig. 3a,b). DNCs also expressed many of these factors, albeit at much lower transcript levels.

FRCs also regulate LN vasculature[20]. They expressed vascular endothelial growth factor (VEGF)-A as previously described, and we detected transcripts for several other angiogenic regulatory molecules including VEGF-C, angiopoietin-related protein 2, hepatocyte growth factor, gremlin 1, and pigment epithelium-derived factor (SerpinF1) (Fig. 3a). DNCs shared expression of some of these factors, while ECs expressed relevant receptors (Fig. 3a). ECs produced fibroblastic growth factors including platelet derived growth factors A, B, C, and D, suggesting a dynamic co-dependence between FRCs and ECs.

FRCs dominated chemokine production, though here too DNCs resembled FRCs (Fig. 3b). As expected, FRCs produced high levels of CCL19 and CCL21a transcripts, while relevant hematopoietic subsets expressed CCR7 (Fig. 3b). While little CCL19 mRNA was detected in ECs, in agreement with past reports[2], BECs showed substantial expression of CCL21a (Fig. 3b). Surprisingly, we found that FRCs strongly transcribed CXCL13, a B cell chemoattractant reportedly restricted to follicular dendritic cells (FDCs) and a minor MAdCAM-1$^+$ population of marginal reticular cells (MRCs). We did not detect FDCs in our cell preparations, based on expression of canonical FDC markers CD21, CD35, and Fcε receptor II (Supplementary Fig. 3a,b). We determined whether MRCs were responsible for observed CXCL13 expression by sorting MAdCAM-1$^-$ FRCs and MAdCAM-1$^+$gp38$^+$CD140a$^+$CD31$^-$ MRCs. Both subsets showed comparable expression of CXCL13 by PCR (Supplementary Fig. 3c). Consistent with the PCR data, MAdCAM1$^-$ and bulk SLN FRCs had similar CXCL13 transcript levels as measured by microarray (Supplementary Fig. 3d).

FRCs transcribed other chemokines such as CCL2 and CCL7, which may facilitate the recruitment or organization of receptor-expressing memory T cells and DCs (Fig. 3b). FRCs were the primary source of the lymphocyte chemoattractant CXCL12, with more than twice as much expression as BECs and DNCs. LECs uniquely expressed CCL20 (Fig. 3b), which is suggested to promote egress of activated T cells from LNs[21]. Memory T cells and B cells expressed the highest levels of CCR6 transcript, suggesting that CCL20 may be relevant to these populations. Together, these data imply that LNSCs play a significant role in regulating immune cell recruitment to and localization within secondary lymphoid organs (SLOs).

Integrins help shape cell-cell and cell-ECM interactions; we therefore examined LNSC integrin expression profiles. While subsets shared expression of certain integrin chains such as integrins α1, α5, and β1, expression of other chains followed a more restricted pattern (Fig. 3c). In fact, DNCs expressed little integrin α2 in contrast to FRCs, LECs, and BECs, and this was also evident at the protein level (Fig. 3c, Supplementary Fig. 2c,d). Meanwhile,

FRCs and DNCs shared expression of the integrin α11 and β5 chains, while DNCs uniquely expressed integrin chains α7, α8, and α4 among LNSCs.

These data suggest that stromal subsets support hematopoietic cells as well as each other via complex regulatory networks.

Identification of new conduit network components

FRCs create unique, yet poorly studied conduits that deliver small, lymph-borne factors to the cortex faster than filtration through cell-dense tissue would allow. At the conduit center lies a collagen-rich core, enveloped by a microfibrillar zone containing fibrillins and the ER-TR7 antigen[9] **(**Supplementary Fig. 4a**)**. Surrounding the microfibrillar zone is a basement membrane ensheathed by FRCs[9]. Since FRCs were enriched for genes encoding ECM-receptor interactions **(**Fig. 2d**)**, their transcription and secretion of conduit components were examined.

In addition to collagens I and IV[9], FRCs expressed transcripts for collagens III, V, VI, XIV, and XVI (Fig. 4a). DNCs strongly resembled FRCs in expression of these molecules. Collagen XV was most highly expressed by BECs, while LECs and DNCs shared collagen XII expression. Immunofluorescence (IF) microscopy revealed collagen XIV ensheathment by ER-TR7, placing it within the collagen core (Fig. 4c, Supplementary Fig. 4b, and Supplementary Fig. 5). Collagen VI, however, mostly colocalized with ER-TR7, localizing it to the microfibrillar zone (Fig. 4d, Supplementary Fig. 4f, and Supplementary Fig. 6).

FRCs can regulate conduit structure and organization through secretion of molecules such as small leucine-rich proteoglycans (SLRPs). SLRPs regulate collagen fibrillogenesis, bridge collagen I fibrils to the basement membrane, and interact with growth factors[22]. FRCs highly expressed the SLRPs lumican, fibromodulin, osteoglycin, decorin, biglycan, and prolargin (Fig. 4a). By IF microscopy, decorin, biglycan, and fibromodulin were surrounded by ER-TR7 and localized to the conduit core (Fig. 4c, Supplementary Fig. 4c-e, and Supplementary Fig. 7-8).

The conduit basement membrane contains laminins 8 (α4β1γ1) and 10 (α5β1γ1)[9], which are expressed by all LNSCs (Fig. 4a). FRCs expressed laminin chains α2, α3, and γ3, suggesting that other laminins may also contribute to conduit structure and function (Fig. 4a). FRCs expressed transcript for the glycoprotein vitronectin, which promotes cell adhesion and spreading, inhibits the membrane attack complex of the complement system, and prevents plasminogen activator inhibitor-ECM interactions[23]. Vitronectin has primarily been observed in B cell follicles, but also exhibits a reticular pattern in the T-zone[24]. We found that vitronectin decorated the surface of ER-TR7$^+$ fibers, forming cage-like structures at conduit branch points (Fig. 4e, Supplementary Fig. 4g, and Supplementary Fig. 9), and was enwrapped by α-SMA$^+$ FRCs, localizing it to the basement membrane (Supplementary Fig. 4h).

LNs undergo dramatic expansion and contraction during immune responses, often in a matter of hours, suggesting extensive remodeling of ECM to accommodate these changes. Matrix metalloproteinases (MMPs) are important for turnover of ECM in other organs[25],

and are expressed by LNSCs (Fig. 4a). MMP2 and MMP3 transcript levels were highest in FRCs and DNCs, whereas FRCs, DNCs, and LECs expressed substantial quantities of MMP9 and MMP14 transcripts (Fig. 4a). In contrast, MMP15 was most highly expressed by BECs. LECs and BECs also expressed higher levels of a disintegrin and metallopeptidase domain 10 mRNA and protein than FRCs or DNCs (Fig. 4a,b). FRCs produced large amounts of transcripts for molecules involved in matrix and elastic fiber assembly including lysyl oxidase (LOX), LOX-like 1, microfibrillar associated protein (MFAP)-2, MFAP-5, and fibulin 1 (Fig. 4a). These data describe a more complex picture of conduit structure and ECM maintenance by FRCs than was previously realized.

Organ-specific specialization of fibroblastic stroma

FRCs are thought to be highly specialized to the lymphoid microenvironment, but in-depth comparisons to other fibroblast populations have not been performed. Skin fibroblasts (SFs, $CD45^{-}gp38^{+}CD31^{-}CD140a^{+}$), sorted to high purity from 5 mice per replicate (Supplementary Fig. 10a-c), and MTS-15^{+} thymic fibroblasts (ThFs) were analyzed. Population distances were computed on differentially expressed probes using PCA, correlation scores, and Euclidean distances (Fig. 5a-c). LN FRCs were most similar across all metrics. PCA and Euclidean distance suggested that FRCs were more like SFs, while correlation scores implied higher concordance between SFs and ThFs.

Genes that distinguish SLN FRCs, ThFs, and SFs in pairwise comparisons (δ=1.0 (adjusted FC≥2); $P<0.05$ for differences in EV), listed in Supplementary Table 3, were mapped to KEGG pathways. Enriched pathways (Benjamini $P<0.05$) were displayed on P value by P value plots, and five biologically interesting hits were labeled (Fig. 5d). FRC-specific probes were uniquely enriched in the cytokine-cytokine receptor pathway, evidenced by this probe's position on the FRC plot (Fig. 5d). Strikingly, FRCs and ThFs were biased towards antigen presentation and contractile ability (Fig. 5d). SFs showed enrichment in classical fibroblast functions involving ECM-receptor interactions (Fig. 5d).

FRCs showed increased expression of many components of the MHC class I pathway including antigen processing machinery and canonical and non-canonical MHC class I molecules, relative to SFs (Supplementary Fig. 10d). ThFs, SLN ECs, and immune cells also showed higher levels of such transcripts, suggesting that lymphoid tissue environments might enhance transcription of these genes. While FRCs expressed some components of the MHC class II pathway more highly than SFs, levels were much lower than in professional antigen presenting cells (Supplementary Fig. 10d).

In addition to presenting self-antigens, FRCs regulate immune cell recruitment to and homeostasis within LNs. While FRCs, SFs, and ThFs produced transcripts for similar chemokines and cytokines, levels were much higher in FRCs (Supplementary Fig. 10d), reflecting functional specialization of these LN residents.

The KEGG analysis suggested that FRCs and ThFs were biased towards contractile ability relative to SFs (Fig. 5d). FRCs express α-SMA, and their contractility has been demonstrated using a wrinkle assay[2]. While FRCs expressed much higher levels of α-SMA and smooth muscle myosin light chain than SFs and ThFs (Supplementary Fig. 10d), both

FRCs and ThFs produced substantially more transcript for other smooth muscle-associated genes (Supplementary Fig. 10d). Consistent with their expression profile, FRCs exhibited strong contractile function compared with NIH3T3 fibroblasts, on par with C2C12 myoblasts **(**Fig. 5e**)**.

Production and maintenance of ECM are fundamental characteristics of fibroblasts. KEGG pathway analysis suggested that SFs were most specialized to these functions (Fig. 5d). Interestingly, while all fibroblastic populations shared expression of most ECM components, FRCs uniquely expressed certain ECM or matrix regulatory molecules, or shared expression with ThFs (Supplementary Fig. 10d). In contrast to SFs, FRCs and ThFs highly transcribed MMP9. FRCs also most highly expressed the ECM remodeling molecules MMP23 and heparanase, and the conduit components vitronectin and fibromodulin (Supplementary Fig. 10d).

Together, these data demonstrate that FRCs shared a surprising number of characteristics with their skin and thymic counterparts, but they are nonetheless specialized to their unique microenvironment.

Cadherin-11 identifies cell-cell junctions between FRCs

FRCs interact closely with each other as they ensheath the reticular fibers that they secrete **(**Supplementary Fig. 11**)**, however, little is known about these junctions. We examined LNSC expression of candidate cell adhesion molecules, and observed high expression of cadherin-11 by FRCs (Fig. 6a). Cadherin-11 is a member of the calcium-dependent cadherin family of adhesion molecules[26]. Expression of cadherin-11 in the LN has previously been observed[27]; however, its specific localization was unknown. Interestingly, transcripts for cadherin-11 were also observed in SFs and ThFs (and DNCs to a lesser extent), reflecting a common mesenchymal origin of these cells[26] (Fig. 6a).

We confirmed surface expression of cadherin-11 on freshly isolated FRCs by flow cytometry (Fig. 6b). In accordance with the microarray data, ECs showed little to no expression of cadherin-11, DNCs showed some expression, and hematopoietic cells were distinctly negative (Fig. 6b).

Cadherin molecules form homotypic interactions, binding cadherins of the same type in adjacent cells and interacting laterally within a single cell[26]. Cadherin-11 localization was evaluated on *in vitro* expanded FRCs, which were found to maintain surface expression of this protein (Fig. 6c). Cadherin-11 was observed by IF microscopy in junctions between adjacent FRCs (Fig. 6d), as shown in fibroblast-like synoviocytes[26]. The specific expression of cadherin-11 in FRCs suggests that it may contribute to FRC-FRC interactions.

DN stromal cells are contractile pericytes

Several groups have reported the existence of DNCs[2,6,7], which comprise 5-10% of LNSCs yet possess unknown lineage, localization, phenotype and function. It is unclear whether DNCs encompass highly tolerogenic extrathymic AIRE-expressing cells (eTACs)[5]. Unlike eTACs, DNCs do not express EpCAM[6], but were the only LNSC subset to transcribe even low levels of AIRE[6,7], though protein was not observed[6].

DNCs uniquely lack TLR3 expression[6], and show differential expression of peripheral tissue-restricted antigens[6]. DNCs lack many surface proteins characteristic of other LNSCs. As part of our sorting strategy, we chose to further define DN cells as $CD44^{-}$, as we found that this combination excluded contaminating $CD45^{lo}CD44^{+}$ cells.

Throughout our analysis, DNCs resembled FRCs. DNCs were compared to other LNSCs using 2-class-EV versus FC plots. DNCs and FRCs differed (FC≥2) in expression of 834 probes (Fig. 7a). In contrast, DNCs and ECs varied in expression of more than 1,880 probes (Fig. 7b,c). Thus, the transcriptional profiles of DNCs and FRCs were similar despite strong differences in surface phenotype[6]. DN-specific and FRC-specific probes were identified (δ=1.0 (adjusted FC≥2); P<0.05 for differences in EV; SLN DNCs vs SLN FRCs) (Supplementary Table 4). MLN DNCs were found to closely resemble SLN DNCs in expression of these genes (**data not shown**). Using DAVID, FRC-specific probes showed enrichment in cytokine-cytokine receptor interactions. In contrast, DNCs highly expressed genes for structural and contractile functions, with KEGG profiles reminiscent of cardiomyocytes and smooth muscle cells (SMCs) (Fig. 7d). Genes important for smooth muscle contraction, including actin subtypes and myosin chains were examined (Fig. 7e). Of these genes, *Actg2* and *Myh11* are described as SMC-specific[28], while others are common to multiple cell types. Strikingly, while α-SMA is often used as a surrogate marker for FRCs, DNCs expressed the highest levels of transcript for this protein (Fig. 7e).

We next sought potential markers to dissect this conceivably heterogenous bulk-negative population, in hopes of assigning it a LN microniche and likely function. Two candidates arose: calponin-1 (CNN1) and integrin α7 (Fig. 7f). Calponin-1 is a SMC-specific actin-associated protein and a major regulator of force production in contractile cells[28]. Integrin α7 pairs with ß1 to bind basement membrane laminins 1, 2 and 4, and is important for linking muscle fibers to ECM[29]. Indeed, sorted DNCs only grew in culture when supplemented with Matrigel (a gel consisting of basement membrane proteins), and formed strong contractile attachments to the matrix (Fig. 7g).

Antibodies to CNN1 and ITGA7 identified DNCs as pericyte-like cells, surrounding some medullary and cortical vessels (Fig. 7h,i). There were no apparent morphological differences between vessels with or without these cells. CNN1 also identified an elongated, subcapsular DN subset limited to the medullary face of the LN. This subset was not stained by anti-ITGA7 (**data not shown**). By flow cytometry, however, it was apparent that CNN1 identified a small minority (<5%) of DNCs, while anti-ITGA7 stained >50% of DNCs (Supplementary Fig. 12) suggesting that pericytes were the major population comprising DNCs. These data identify most DNCs as fibroblastic, contractile pericytes, which we term $ITGA7^{+}$ pericytes (IAPs).

Inflammation triggers transcriptional changes in LNSCs

FRCs, LECs, BECs, and IAPs are positioned at key sites throughout the LN to encounter lymph-borne molecules, and their steady-state transcriptional profiles suggest they are poised to respond to inflammatory or infectious insults. To investigate stromal cell responses to inflammation and ongoing immune responses, we transferred 1.5×10^{6} OT-I T cells intravenously to 5 week old C57BL/6 mice. 18 hours after T cell transfer, mice received 30

μg *Escherichia coli* (O127:B8) lipopolysaccharide (LPS) and 500 μg ovalbumin (OVA) intravenously **(**Supplementary Fig. 13a**)**. Using 5-6 mice per replicate, FRCs, LECs, and BECs were isolated from SLNs and sorted to high purity 12 hours post-LPS and OVA injection (12 h FRCs, 12 h LECs, and 12 h BECs) **(**Supplementary Fig. 13b**)**. Due to the rarity of IAPs, this subset was not sorted for further analysis.

Treatment markedly changed the transcriptional profiles of FRCs, LECs, and BECs, demonstrated by hierarchical clustering of 373 probes that were differentially expressed (FC>2, $P<0.05$) between 12 h stromal subsets and corresponding untreated counterparts (Fig. 8a). 113 differentially expressed probes were identified ($\delta=1.0$ (adjusted FC≥2); $P<0.05$ for differences in EV; 12 h SLN FRCs vs untreated SLN FRCs, etc.) for further study (Supplementary Table 5). Probes upregulated in 12 h FRCs and 12 h BECs showed substantial enrichment for the KEGG antigen processing and presentation pathway, in contrast to probes upregulated in 12 h LECs (Fig. 8b). Probes downregulated following treatment of mice did not show enrichment for particular KEGG pathways.

Projection of the 113 differentially expressed probes onto FC vs *P* value plots of stromal subsets from 12 h and untreated mice resulted in similar probe distributions, though FRCs appeared to respond most strongly at this time point as FCs were generally largest within this subset (Fig. 8c). Consistent with an inflammatory milieu, 12 h FRCs demonstrated enhanced expression of acute phase response genes including serum amyloid A 3; alpha-2-macroglobulin; and serine (or cysteine) peptidase inhibitor, clade A, member 1B; while all three subsets showed increased mRNA for the inflammatory chemokines CCL5 and CXCL9 (Fig. 8c). In addition, transcripts for numerous IFN- or TLR4-inducible or regulatory genes such as interferon regulatory factor 7[30], lymphocyte antigen 6 complex, locus A[31], and lipocalin 2 (LCN2)[32] were upregulated in 12 h stroma (Fig. 8c). Nuclear receptor subfamily 1, group D, member 1, a negative regulator of TLR4 signaling[33], mRNA levels were diminished in 12 h stromal subsets. We observed that while not part of the 113 probe list, IL-7 and IL-33 transcripts were also significantly upregulated in 12 h FRCs (2.6-fold, $P=0.003$; 1.9-fold, $P=0.001$). Transcripts for a variety of ECM-associated genes such as MMP9; periostin; collagen, type VI, α6; and laminin α2 were significantly downregulated in FRCs following treatment of mice, and this trend was also observed to a lesser degree in LECs and BECs (Fig. 8c).

In accordance with the KEGG pathway analysis, we found that 12 h FRCs and 12 h BECs upregulated multiple components of the MHC class II presentation pathway including MHC class II molecule chains (H2-Aα, H2-Aβ1, and H2-Eβ1), the invariant chain (CD74), cathepsin S, H2-DMα, and H2-DMβ2 (Fig. 8c). Furthermore, 12 h FRCs also exhibited significantly increased expression of legumain (Fig. 8c), Using flow cytometry, we investigated surface expression of MHC II on SLN FRCs, LECs, BECs, and DNCs isolated from mice 18 hours after treatment (18 h mice) (Fig. 8d,e). Following treatment, surface expression of MHC II was significantly increased on FRCs, LECs, and BECs, though not on DNCs. Consistent with the microarray data, FRCs and BECs demonstrated larger increases in MHC II expression than LECs (Fig. 8d,e).

LCN2 is a multifaceted, LPS-inducible molecule that has been implicated in host-defense to *Escherichia coli*, *Klebsiella pneumoniae*, and *Mycobacterium tuberculosis*[32]. Given the substantial increase in FRC, LEC, and BEC expression of LCN2 following treatment (17.5-fold, 3.5-fold, and 4.8-fold respectively), we stained SLN sections from untreated and 18 h mice using antibodies to LCN2, desmin (FRCs), lymphatic vessel endothelial hyaluronan receptor 1 (LYVE-1, LECs), and peripheral node addressin (pNAd, BECs) (Fig. 8f). In contrast to FRCs, LECs, and BECs in SLN sections from untreated mice, LCN2 could be detected in all three stromal subsets 18 hours after treatment (Fig. 8f). In agreement with previous reports[32], LCN2 could also be observed in desmin^{-}, LYVE-1^{-}, and pNAd^{-} cells, likely of hematopoietic origin (**data not shown**).

These data reinforce the notion that LNSCs are poised to respond to inflammatory or infectious triggers and may contribute as active participants during ongoing immune responses.

DISCUSSION

The LN conduit network is a complex molecular sieve that rapidly delivers low molecular weight lymph-borne molecules deep into the cortex[9]. This unique capacity for size-exclusion is key to conduit function, yet its molecular basis is poorly understood. Dissection of ECM expression data from FRCs revealed a potential mechanism for regulating conduit structure and function.

In addition to collagen I, which assembles into long fibrillar chains, providing tensile strength, we found that the collagen core contained collagen XIV, which cross-links collagen I, limiting fibril diameter by preventing lateral binding of adjacent fibrils[34]. The SLRP decorin, also highly expressed in the conduit core, is another key regulator of fibril diameter[35]. Lastly, LOX covalently cross-links collagen I-collagen XIV bonds, locking the low-diameter arrangement[36]. Macromolecular diffusion studies report that collagen fibrils possess pore-type permeability dependent on tertiary and quaternary structure[37]. Tight regulation of fibril diameter and packing conceivably control pore size; dysregulation could impair small-molecule delivery to the LN parenchyma and alter the structural integrity of the network. We suggest that size-exclusion in conduits is a property of the type I collagen core tightly regulated by collagen XIV and SLRPs. Ongoing studies will define the roles of these factors in regulating fibril density and diameter in LNs.

LNSC transcriptional profiles suggest that these cells may be poised to respond to lymph-borne infectious or inflammatory cues. While LNSCs lacked transcript for NALP3, part of the inflammasome that recognizes influenza and adenovirus[38], FRCs and DNCs produced more interferon-inducible transmembrane protein (IFITM)-1 transcript than other profiled populations. Furthermore, LNSCs expressed more IFITM-2and IFITM-3 transcript than hematopoietic cells. IFITM-1, IFITM-2, and IFITM-3 have recently been implicated in host defense to influenza, West Nile virus, and Dengue virus[39].

We have previously shown that ligation of TLR3, another viral recognition receptor, decreased FRC activation of T cells[6]. LNSC exposure to infectious agents is hypothesized to

preserve LN architecture by promoting stromal resistance to immune-mediated destruction[6,40].

We found that FRCs, LECs, and BECs, all of which express TLR4 in the steady-state, responded vigorously to the onset of inflammation by upregulating expression of interferon and/ or TLR4 inducible or regulatory genes, acute phase response genes, inflammatory chemokines CCL5 and CXCL9, and key components of the MHC class II antigen processing and presentation pathway. Notably expression of MHC class II molecule chains (H2-Aα, H2-Aβ1, and H2-Eβ1), the invariant chain (CD74), cathepsin S, H2-DMα, and H2-DMβ2 was increased in FRCs and BECs following the onset of inflammation. FRCs also upregulated legumain. Surface MHC II expression was indeed increased on FRCs, LECs, and BECs 18 hours after injection of LPS and OVA, while levels remained unchanged on DNCs. LNSC presentation of antigens via MHC II may contribute to the induction of $CD4^+$ T cell tolerance or the generation of regulatory T cells in inflammatory settings or during chronic immune responses. Future studies will elucidate the role that the MHC II antigen processing and presentation pathway plays in LNSCs under inflammatory conditions. FRCs, LECs, and BECs were also observed to produce LCN2, a potent anti-microbial iron-binding molecule[32], following the onset of inflammation. LNSC secretion of Lcn2 may limit bacterial expansion during early stages of infection by decreasing the availability of iron[32].

While FRCs are SLO residents, similarly specialized fibroblasts appear at sites of chronic inflammation (tertiary lymphoid organs; TLOs) and in tumors, where they support LN-like environments[13,14]. These FRC-like cells are often associated with poor clinical outcomes[13,14]. Controlling TLO development is therefore an important therapeutic aim; however, fibroblastic populations from different tissues have not been systematically compared. We examined FRC, ThF, and SF transcriptomes to study lymphoid organ fibroblast specialization. Despite sharing many characteristics, each population exhibited a distinctive profile. Relative to SFs, both FRCs and ThFs were better equipped for antigen presentation and contractility. Exposure to immune mediators and lymph flow[41] likely regulate the FRC transcriptome. FRCs were uniquely enriched for cytokine-cytokine receptor interactions, demonstrating further immune-related specialization.

In contrast to interstitial fibroblasts, FRCs interact closely with each other along the conduits that they ensheath[42], however, little is known about these cell-cell contacts. We report that cadherin-11 localizes to junctions between FRCs. Cadherin-11 transcripts were also observed in ThFs and SFs, reflecting a common mesenchymal origin. Cadherin-11 upregulation is associated with increased division, adhesion, bone infiltration, inflammatory cytokine production, and altered ECM production by fibroblast-like synoviocytes in rheumatoid arthritis[26,43]. Future studies will determine whether cadherin-11 signaling in FRCs regulates similar processes.

LNSCs interact closely with hematopoietic cells. Accordingly, we examined LN stromal and hematopoietic niches for novel aspects of crosstalk. A striking finding was shared stromal expression of many genes thought to be subset-restricted. FRCs, and to a lesser extent DNCs, produced transcripts for cytokines and chemokines that may act on memory T cells, DCs, B cells, macrophages, and NK cells, likely contributing to their recruitment,

organization, and survival. FRCs expressed the highest levels of FLT3L transcript among profiled stromal and hematopoietic subsets, suggesting a novel role in maintaining LN-resident DCs, similar to thymic stroma[44]. Meanwhile, CCL20 expression by LECs may contribute to steady-state egress of memory T cells or B cells. While FRCs produced substantial CCL19 and CCL21a transcript, as previously reported[2], lower transcript levels were observed in other LNSCs. In addition, both FRCs and LECs transcribed IL-7, in contrast to earlier reports[2]. Furthermore, FRCs, BECs, and DNCs highly expressed the homeostatic chemokine CXCL12. Unexpectedly, we observed CXCL13 expression in FRCs. Microscopy confirmed CXCL13 localization to B cell follicles, where rare FRCs ensheath sparse conduits[45]. 11.6±8.2% of CXCL13^{bright} areas were associated with desmin^{+} FRCs surrounding ER-TR7^{+} conduits (data not shown), suggesting that B-zone FRCs may form a discrete CXCL13-expressing subset. Alternatively, T-zone FRCs may also produce CXCL13 transcript, but protein synthesis may be tightly regulated.

Notably, our data suggest that FRCs contribute to EC maintenance. In addition to confirming FRC expression of VEGF-A[20], our analysis revealed FRC-restricted expression of transcripts for other angiogenic and lymph-angiogenic molecules including VEGF-C, HGF, and gremlin 1[46], while FRCs, LECs, and DNCs shared expression of ANGPTL4. Importantly, BECs and LECs produced transcripts for relevant receptors. Thus, it is likely that in addition to regulating immune cell homeostasis, FRCs promote the survival and proliferation of ECs.

Little is known about the DN niche. DNCs most closely resembled FRCs in terms of global gene expression and cytokine, chemokine, and growth factor production. DN-specific probes were enriched for contractile function relative to FRCs, and cultured DNCs formed elongated networks that strongly contracted 3D collagen matrices. In vivo, we found that ITGA7 was an effective surface marker for >50% of DNCs, subsequently identified as highly contractile cells that we named IAPs. Further studies are needed to elucidate any developmental relationship between IAPs and FRCs, and whether IAP-ensheathed vessels demonstrate functional specialization.

This study aimed to provide the first comparative transcriptome analysis of lymphoid organ stroma. The data simultaneously support and extend previous findings while providing ready access to a comprehensive database of molecular determinants expressed by LNSCs. By comparing stromal data to data gathered for hematopoietic cells, plausible webs of interaction became apparent. As an immunological resource, this expression patterning analysis suggested that LNSCs are closely involved in many facets of immune regulation, structural support, and stromal cell homeostasis, providing supportive data for many new avenues of study.

METHODS

Mice

Per ImGen standard operating protocol (SOP), all mice used were five week old male C57BL/6 mice from the Jackson Laboratory, shipped one week prior to use and maintained under specific pathogen free conditions. Rag2$^{-/-}$OT-I T cell receptor-transgenic mice were

obtained from Taconic and bred at the Dana-Farber Cancer Institute. Mice were cared for under institutional and National Institutes of Health guidelines. Experiments were carried out with approval of the Research Animal Care subcommittee at the Dana-Farber Cancer Institute.

Induction of inflammation

1.5×10^6 OT-I T cells were transferred intravenously to C57BL/6 mice. 18 hours later mice received 30 μg LPS from *E. coli* (serotype 0127:B8, L3129, Sigma-Aldrich) and 500 μg OVA (A5503, Sigma-Aldrich) intravenously. SLNs were collected 12 hours after LPS and OVA injection for sorting of FRCs, LECs, and BECs for microarray analysis. SLNs were collected 18 hours after LPS and OVA injection for analysis of MHC II and Lcn2 protein expression.

Antibodies and conjugates

We used: anti-CD45 (clone 30-F11, Biolegend), Ter119 (Biolegend), anti-CD31 (clone MEC13.3, Biolegend); anti-gp38 (clone 8.1.1, purified in house from a hybridoma obtained from the Developmental Studies Hybridoma Bank); anti-CD140a (clone APA5, eBioscience); anti-MAdCAM-1 (MECA-367, eBioscience); anti-Cadherin-11 (clone 13C2) and MOPC21 (kind gifts from Michael Brenner); anti-mouse-I-A/I-E (clone M5/114.15.2, Biolegend); anti-mouse-CD44 (clone IM7, eBioscience), polyclonal-anti-collagen VI (ab6588, Abcam); polyclonal-anti-collagen XIV (generous gift from Manuel Koch); anti-vitronectin (ab28023, Abcam); ER-TR7 (ab51824, Abcam); anti-α-smooth muscle actin (clone 1A4, Sigma-Aldrich); anti-ITGA7-FITC (clone 3349908, R&D Systems); anti-CNN1 (clone EP7984, Epitomics); polyclonal-anti-fibromodulin (batch LF-150), polyclonal-anti-mouse-decorin (batch LF-113[47]), and polyclonal-anti-mouse-biglycan (batch LF-159[47]) (kind gifts from Larry Fisher); polyclonal-anti-desmin (ab15200, Abcam); anti-pNAd-biotin (clone MECA-79, Biolegend), anti-LYVE-1-A488 (clone ALY7, eBioscience); polyclonal-anti-LCN2 (AF1857, R&D Systems); anti-hamster-A488 (A-21110, Invitrogen); anti-rat-A647 (A-21247, Invitrogen); anti-rabbit-A488 (A-11034, Invitrogen); anti-rabbit-IgG-A647 (A-31573, Invitrogen); anti-rabbit-A555 (A-31572, Invitrogen); anti-goat-IgG-A488 (A-11055, Invitrogen); anti-goat-IgG-biotin (A-10518, Invitrogen); anti-mouse-IgG1-biotin (550331, BD); anti-mouse-IgG (A-11029, Invitrogen); polyclonal anti-mouse ADAM10 (AB946, R&D); DAPI (D3571, Invitrogen); TRITC-phalloidin (R415, Invitrogen); SA-A555 (S-32355); and SA-A488 (S-32354, Invitrogen).

Cell enrichment and sorting

Cells were prepared according to ImmGen SOP (www.immgen.org). Skin-draining (inguinal, axillary, and brachial) and mesenteric LNs were isolated from 10-30 C57BL/6mice, digested, enriched for $CD45^-$ stroma, and sorted as previously described[6,48]. For skin fibroblasts, ears from 5 mice per group were placed in ice cold RPMI, 2% FBS, then split and sliced using a razor blade, and digested as described[6]. Red blood cells were lysed (140 mM NH_4Cl, 17 mM Tris-base, pH 7.4) and cells were stained and sorted (single round of sorting) directly into TRIzol, using a FACSAria (100 μm nozzle, 20 psi). Dead cells were excluded using propidium iodide (5ng/mL). Purity was assessed by sorting cells into FACS

buffer (2% FBS, 2mM EDTA, and PBS) and immediately analyzing samples using the FACSAria. RNA was isolated as described[49].

Microarray hybridization and data normalization

Isolated RNA was amplified and prepared for hybridization to the Affymetrix MoGene 1.0 ST array using the GeneChip Whole Transcript (WT) Sense Target Labeling Assay in accordance with manufacturer's instructions. Raw data was normalized using the robust multichip average algorithm in the "Expression File Creator" module (GenePattern).

Expression value probabilities

Thresholds for likelihood of positive gene expression were determined from the distribution of expression across the microarrays. Because the ST1.0 arrays do not contain reliable negative controls, a Gaussian Mixture Model was used to determine probabilistic thresholds of expression, an approach initially validated by comparing parallel datasets obtained from the same B and T lymphocyte RNAs[49]. Probabilities of components within the model were combined to arrive at a single probability of expression. Thresholds were calculated for each sample, and the distribution of cutoffs was examined to determine whether a single value could be applied to all ImmGen samples. The post-normalization expression value of 120, corresponding to a 95% probability of expression, was used as the standard cutoff for gene expression for most populations within ImmGen.

Population distance measurements

PCA was performed on expressed probes using the "ImmGen Population PCA Plot" module in GenePattern. PCA reduces the complexity of multi-dimensional data into PCs. Each PC is uncorrelated with earlier PCs, to account for maximal variability among populations. This module identified and used the 15% most differentially expressed probes across populations for PCA. Data was $\log_2$ transformed, and row- and column-normalized prior to PCA. The 15% most variable probes were identified in an unsupervised manner: for all expressed probes (MEV>120 for any subset), the module:

1. Uses replicate values to compute the standard deviation (SD) within each population and averages these values to generate a single SD value that reflects variability within each cell type (SD_within).
2. Uses mean expression values to calculate the SD across all cell populations (SD_across).

Probes were ranked according to the following ratio: SD_across/SD_within. Those probes with the highest ratio were determined to be the most variable, and the top 15% of these were used. The first three PCs were used as coordinate-axes onto which samples were projected. Pearson correlation coefficients and Euclidean distances were calculated using the same probes. Data was $\log_2$ transformed and row-standardized. Correlation and distance values were computed using R. Heatmaps were generated using the "HeatMapImage" module (GenePattern).

Hierarchical clustering analysis

Using the "Multiplot" module (GenePattern), differentially expressed probes were identified (FC>2 in at least one pair-wise population comparison, EV>120 for at least one population), then clustered (Pearson's correlation and average-linkage) using the "Hierarchical Clustering" module (GenePattern). Data were $\log_2$ transformed, row-centered and row-normalized, then visualized using the "Hierarchical Clustering Viewer" module (GenePattern).

Stromal gene signature determination (delta score analysis)

The "Delta Score" module (GenePattern) was used to identify stromal cell specific signatures in a pair-wise manner. For two populations, ***a*** and ***b***, effective differential expression was defined as:

$$\delta\,(a,b) = log_2\left(\frac{\mu_a}{\mu_b}\right) - (\sigma_a + \sigma_b)^2$$

where $\boldsymbol{\mu}$ and $\boldsymbol{\sigma}$ are the geometric mean and geometric standard deviation, respectively, of the two populations. The ratio in the first term represents the FC between the class means of ***a*** and ***b***. This value was $\log_2$ transformed (so powers of 2 correspond to FCs). FC values are penalized for noise within replicates by subtracting the square of the sum of the geometric standard deviations of both populations. The resulting delta score (δ) reflects noise-adjusted differences between the two populations. δ=1 corresponds to an adjusted FC≥2, δ=2 corresponds to an adjusted FC≥4, and so on. Lists of differentially expressed probes were combined for subsequent analysis using Excel.

Probes subsequently identified as significantly different in expression using a T-test (P<0.05) were used ("Multiplot" module of GenePattern).

Analysis of functional enrichment within gene signatures

Population-specific lists were analyzed using the Functional Annotation Tool of the NIAID's DAVID (http://david.abcc.ncifcrf.gov/)[16]. Lists were uploaded as "Official Gene Symbols" for *Mus musculus*. Background was set to the MoGene-1_0-st-v-1 chip. Within the "Pathways" option, the "KEGG_Pathway" chart was selected. "Count" requirements for genes were set to 0 and "EASE" score was set to 1. Top ranked or biologically significant hits were displayed with multiple hypothesis corrected (Benjamini) *P* values.

Other general microarray analysis details

For bar graph and heatmap depiction of genes for which multiple probes exist, a single representative probe (that is closest to the mean in Euclidean distance) was selected for visualization.

Immunofluorescence microscopy

LNs were snap frozen in OCT compound. For ITGA7,CNN1, and LCN2 staining, LNs were fixed in 4% PFA for 4 hours and then 30% sucrose overnight prior to freezing. 7.5 μm

sections were cut and blocked using FcR block (clone 2.4G2) and 2% BSA prior to staining with primary and secondary antibodies. For fibromodulin staining, sections were pre-treated with Chondroitinase ABC (Sigma) for 1 hour at 37°C. For cadherin-11 staining of cultured FRCs, 2.5×10^4 cells were plated overnight on fibronectin (33016-015, Invitrogen) coated coverslips. Cells were blocked as above and incubated with primary antibodies. Cells were fixed using 4% PFA, permeablized with 0.2% Triton-X-100 (T-9284, Sigma), and then incubated with secondary conjugates. Sections were visualized using a laser scanning confocal microscope (Leica SP5X), and analyzed with ImageJ (NIH) and Adobe Photoshop CS.

Electron microscopy

Popliteal LNs were prepared and analyzed as previously described[50].

Flow cytometry

LNs were digested and stained as previously described[6]. For cadherin-11 staining, cells were prepared and stained in EDTA-free HBS with 2% FBS and 1 mM $CaCl_2$. Samples were acquired on a FACSCalibur or FACSAria (BD Biosciences) and analyzed using FlowJo v. 8.7.3.

Contraction assay

C2C12 myoblasts and NIH3T3 fibroblasts were cultured until 70% confluent. FRCs from SLNs were cultured as described[6]. 5×10^5 cells were suspended in 500 μL gel (1 mg/mL rat tail collagen I (BD Biosciences) in αMEM) and seeded into tubular constructs. Images were taken using a Nikon camera, and analyzed with ImageJ, measuring contraction as the width of collagen matrix divided by total tube width.

RT-PCR

RNA extraction, cDNA preparation, and PCR cycling conditions were all as described[6]. Primers (Integrated DNA Technologies): CXCL13F: tggccagctgcctctctc and CXCL13R: ttgaaatcactccagaacacctaca.

Statistics

T-test *P* values were computed using Multiplot (GenePattern). For functional enrichment in gene lists, *P* values were corrected for multiple hypothesis testing using the Benajmini option of the DAVID Functional Annotation Tool. *P* values for the chi-square test with Yates' correction were computed using GraphPad Prism 5. False discovery rate adjusted *P* values were calculated using the "ComparativeMarkerSelection" module of GenePattern, which uses the Benjamini and Hochberg procedure.

Supplementary Material

Refer to Web version on PubMed Central for supplementary material.

Acknowledgements

The authors are thankful to Larry Fisher for providing the decorin, fibromodulin, and biglycan antibodies; to Mark Curry for technical assistance in sorting stromal cell populations; to Joel B. Lewis for fruitful discussions during microarray data analysis; and to eBioscience, Affymetrix, and Expression Analysis for support of the ImmGen Project. Additional thanks to Kai W. Wucherpfennig for critical reading of the manuscript and to the members of the ImmGen Consortium. This work was supported by National Institutes of Health grants R01 DK074500 and P01 AI045757 (to S.J.T.), R01 AI063428-06 (to M.B.), R01 DE019917 (to D.J.M.), GM38903 (to M.E.H. and K.K.), a Benacerraf Postdoctoral Fellowship (to K.K.), a Benacerraf Postdoctoral Fellowship (to V.L.K.), and a Seventh Framework Programme of the European Union (Marie Curie International Outgoing Fellowship 220044 to S.F.G.).

REFERENCES

1. Heng TS, Painter MW. The Immunological Genome Project: networks of gene expression in immune cells. Nat Immunol. 2008; 9:1091–1094. doi:10.1038/ni1008-1091. [PubMed: 18800157]
2. Link A, et al. Fibroblastic reticular cells in lymph nodes regulate the homeostasis of naive T cells. Nat Immunol. 2007; 8:1255–1265. doi:10.1038/ni1513. [PubMed: 17893676]
3. Fletcher AL, Malhotra D, Turley SJ. Lymph node stroma broaden the peripheral tolerance paradigm. Trends Immunol. 2011; 32:12–18. doi:10.1016/j.it.2010.11.002. [PubMed: 21147035]
4. Lee JW, et al. Peripheral antigen display by lymph node stroma promotes T cell tolerance to intestinal self. Nat Immunol. 2007; 8:181–190. doi:10.1038/ni1427. [PubMed: 17195844]
5. Gardner JM, et al. Deletional tolerance mediated by extrathymic Aire-expressing cells. Science. 2008; 321:843–847. doi:10.1126/science.1159407. [PubMed: 18687966]
6. Fletcher AL, et al. Lymph node fibroblastic reticular cells directly present peripheral tissue antigen under steady-state and inflammatory conditions. J Exp Med. 2010; 207:689–697. doi:10.1084/jem.20092642. [PubMed: 20308362]
7. Cohen JN, et al. Lymph node-resident lymphatic endothelial cells mediate peripheral tolerance via Aire-independent direct antigen presentation. J Exp Med. 2010; 207:681–688. doi:10.1084/jem.20092465. [PubMed: 20308365]
8. Pham TH, et al. Lymphatic endothelial cell sphingosine kinase activity is required for lymphocyte egress and lymphatic patterning. J Exp Med. 2010; 207:17–27. doi:10.1084/jem.20091619. [PubMed: 20026661]
9. Sixt M, et al. The conduit system transports soluble antigens from the afferent lymph to resident dendritic cells in the T cell area of the lymph node. Immunity. 2005; 22:19–29. doi:10.1016/j.immuni.2004.11.013. [PubMed: 15664156]
10. Roozendaal R, Mebius RE, Kraal G. The conduit system of the lymph node. Int Immunol. 2008; 20:1483–1487. doi:10.1093/intimm/dxn110. [PubMed: 18824503]
11. Palframan RT, et al. Inflammatory chemokine transport and presentation in HEV: a remote control mechanism for monocyte recruitment to lymph nodes in inflamed tissues. J Exp Med. 2001; 194:1361–1373. [PubMed: 11696600]
12. Itano AA, et al. Distinct dendritic cell populations sequentially present antigen to CD4 T cells and stimulate different aspects of cell-mediated immunity. Immunity. 2003; 19:47–57. [PubMed: 12871638]
13. Kalluri R, Zeisberg M. Fibroblasts in cancer. Nat Rev Cancer. 2006; 6:392–401. doi:10.1038/nrc1877. [PubMed: 16572188]
14. Link A, et al. Association of T-zone reticular networks and conduits with ectopic lymphoid tissues in mice and humans. Am J Pathol. 2011; 178:1662–1675. doi:10.1016/j.ajpath.2010.12.039. [PubMed: 21435450]
15. Reich M, et al. GenePattern 2.0. Nat Genet. 2006; 38:500–501. doi:10.1038/ng0506-500. [PubMed: 16642009]
16. Huang da W, Sherman BT, Lempicki RA. Systematic and integrative analysis of large gene lists using DAVID bioinformatics resources. Nat Protoc. 2009; 4:44–57. doi:10.1038/nprot.2008.211. [PubMed: 19131956]
17. Mackay F, Leung H. The role of the BAFF/APRIL system on T cell function. Semin Immunol. 2006; 18:284–289. doi:10.1016/j.smim.2006.04.005. [PubMed: 16931039]

18. Wei S, et al. Functional overlap but differential expression of CSF-1 and IL-34 in their CSF-1 receptor-mediated regulation of myeloid cells. J Leukoc Biol. 2010; 88:495–505. doi:10.1189/jlb.1209822. [PubMed: 20504948]
19. Watowich SS, Liu YJ. Mechanisms regulating dendritic cell specification and development. Immunol Rev. 2010; 238:76–92. doi:10.1111/j.1600-065X.2010.00949.x. [PubMed: 20969586]
20. Chyou S, et al. Fibroblast-type reticular stromal cells regulate the lymph node vasculature. J Immunol. 2008; 181:3887–3896. [PubMed: 18768843]
21. Liston A, et al. Inhibition of CCR6 function reduces the severity of experimental autoimmune encephalomyelitis via effects on the priming phase of the immune response. J Immunol. 2009; 182:3121–3130. doi:10.4049/jimmunol.0713169. [PubMed: 19234209]
22. Kalamajski S, Oldberg A. The role of small leucine-rich proteoglycans in collagen fibrillogenesis. Matrix Biol. 2010; 29:248–253. doi:10.1016/j.matbio.2010.01.001. [PubMed: 20080181]
23. Schvartz I, Seger D, Shaltiel S. Vitronectin. Int J Biochem Cell Biol. 1999; 31:539–544. [PubMed: 10399314]
24. van den Berg TK, van der Ende M, Dopp EA, Kraal G, Dijkstra CD. Localization of beta 1 integrins and their extracellular ligands in human lymphoid tissues. Am J Pathol. 1993; 143:1098–1110. [PubMed: 7692731]
25. Page-McCaw A, Ewald AJ, Werb Z. Matrix metalloproteinases and the regulation of tissue remodelling. Nat Rev Mol Cell Biol. 2007; 8:221–233. doi:10.1038/nrm2125. [PubMed: 17318226]
26. Chang SK, Gu Z, Brenner MB. Fibroblast-like synoviocytes in inflammatory arthritis pathology: the emerging role of cadherin-11. Immunol Rev. 2010; 233:256–266. doi:10.1111/j.0105-2896.2009.00854.x. [PubMed: 20193004]
27. Moll R, et al. Endothelial and virgultar cell formations in the mammalian lymph node sinus: endothelial differentiation morphotypes characterized by a special kind of junction (complexus adhaerens). Cell Tissue Res. 2009; 335:109–141. doi:10.1007/s00441-008-0700-y. [PubMed: 19015886]
28. Yamamura H, Hirano N, Koyama H, Nishizawa Y, Takahashi K. Loss of smooth muscle calponin results in impaired blood vessel maturation in the tumor-host microenvironment. Cancer Sci. 2007; 98:757–763. doi:10.1111/j.1349-7006.2007.00452.x. [PubMed: 17391313]
29. Mayer U, et al. Absence of integrin alpha 7 causes a novel form of muscular dystrophy. Nat Genet. 1997; 17:318–323. doi:10.1038/ng1197-318. [PubMed: 9354797]
30. Fitzgerald KA, et al. LPS-TLR4 signaling to IRF-3/7 and NF-kappaB involves the toll adapters TRAM and TRIF. J Exp Med. 2003; 198:1043–1055. doi:10.1084/jem.20031023. [PubMed: 14517278]
31. Khan KD, Lindwall G, Maher SE, Bothwell AL. Characterization of promoter elements of an interferon-inducible Ly-6E/A differentiation antigen, which is expressed on activated T cells and hematopoietic stem cells. Mol Cell Biol. 1990; 10:5150–5159. [PubMed: 1697928]
32. Li C, Chan YR. Lipocalin 2 regulation and its complex role in inflammation and cancer. Cytokine. 2011; 56:435–441. doi:10.1016/j.cyto.2011.07.021. [PubMed: 21855366]
33. Fontaine C, et al. The nuclear receptor Rev-erbalpha is a liver X receptor (LXR) target gene driving a negative feedback loop on select LXR-induced pathways in human macrophages. Mol Endocrinol. 2008; 22:1797–1811. doi:10.1210/me.2007-0439. [PubMed: 18511497]
34. Young BB, Gordon MK, Birk DE. Expression of type XIV collagen in developing chicken tendons: association with assembly and growth of collagen fibrils. Dev Dyn. 2000; 217:430–439. doi:10.1002/(SICI)1097-0177(200004)217:4<430::AID-DVDY10>3.0.CO;2-5. [PubMed: 10767087]
35. Danielson KG, et al. Targeted disruption of decorin leads to abnormal collagen fibril morphology and skin fragility. J Cell Biol. 1997; 136:729–743. [PubMed: 9024701]
36. Bailey AJ. Molecular mechanisms of ageing in connective tissues. Mech Ageing Dev. 2001; 122:735–755. [PubMed: 11322995]
37. Gilbert DL, Okano T, Miyata T, Kim SW. Macromolecular diffusion through collagen membranes. Int J Pharm. 1988; 47:79–88. doi:10.1016/0378-5173(88)90217-7.

38. Brennan K, Bowie AG. Activation of host pattern recognition receptors by viruses. Curr Opin Microbiol. 2010; 13:503–507. doi:10.1016/j.mib.2010.05.007. [PubMed: 20538506]
39. Brass AL, et al. The IFITM proteins mediate cellular resistance to influenza A H1N1 virus, West Nile virus, and dengue virus. Cell. 2009; 139:1243–1254. doi:10.1016/j.cell.2009.12.017. [PubMed: 20064371]
40. Mueller SN, et al. Viral targeting of fibroblastic reticular cells contributes to immunosuppression and persistence during chronic infection. Proc Natl Acad Sci U S A. 2007; 104:15430–15435. doi:10.1073/pnas.0702579104. [PubMed: 17878315]
41. Tomei AA, Siegert S, Britschgi MR, Luther SA, Swartz MA. Fluid flow regulates stromal cell organization and CCL21 expression in a tissue-engineered lymph node microenvironment. J Immunol. 2009; 183:4273–4283. doi:10.4049/jimmunol.0900835. [PubMed: 19734211]
42. Lammermann T, Sixt M. The microanatomy of T-cell responses. Immunol Rev. 2008; 221:26–43. doi:10.1111/j.1600-065X.2008.00592.x. [PubMed: 18275473]
43. Chang SK, et al. Cadherin-11 regulates fibroblast inflammation. Proc Natl Acad Sci U S A. 2011; 108:8402–8407. doi:10.1073/pnas.1019437108. [PubMed: 21536877]
44. Kenins L, Gill JW, Boyd RL, Hollander GA, Wodnar-Filipowicz A. Intrathymic expression of Flt3 ligand enhances thymic recovery after irradiation. J Exp Med. 2008; 205:523–531. doi:10.1084/jem.20072065. [PubMed: 18299401]
45. Roozendaal R, et al. Conduits mediate transport of low-molecular-weight antigen to lymph node follicles. Immunity. 2009; 30:264–276. doi:10.1016/j.immuni.2008.12.014. [PubMed: 19185517]
46. Mitola S, et al. Gremlin is a novel agonist of the major proangiogenic receptor VEGFR2. Blood. 2010; 116:3677–3680. doi:10.1182/blood-2010-06-291930. [PubMed: 20660291]
47. Fisher LW, Stubbs JT 3rd, Young MF. Antisera and cDNA probes to human and certain animal model bone matrix noncollagenous proteins. Acta Orthop Scand Suppl. 1995; 266:61–65. [PubMed: 8553864]
48. Fletcher A, et al. Reproducible isolation of lymph node stromal cells reveals site-dependent differences in fibroblastic reticular cells. Frontiers in Immunological Tolerance. 2011
49. Painter MW, Davis S, Hardy RR, Mathis D, Benoist C. Transcriptomes of the B and T lineages compared by multiplatform microarray profiling. J Immunol. 2011; 186:3047–3057. doi:10.4049/jimmunol.1002695. [PubMed: 21307297]
50. Gonzalez SF, et al. Capture of influenza by medullary dendritic cells via SIGN-R1 is essential for humoral immunity in draining lymph nodes. Nat Immunol. 2010; 11:427–434. doi:10.1038/ni.1856. [PubMed: 20305659]

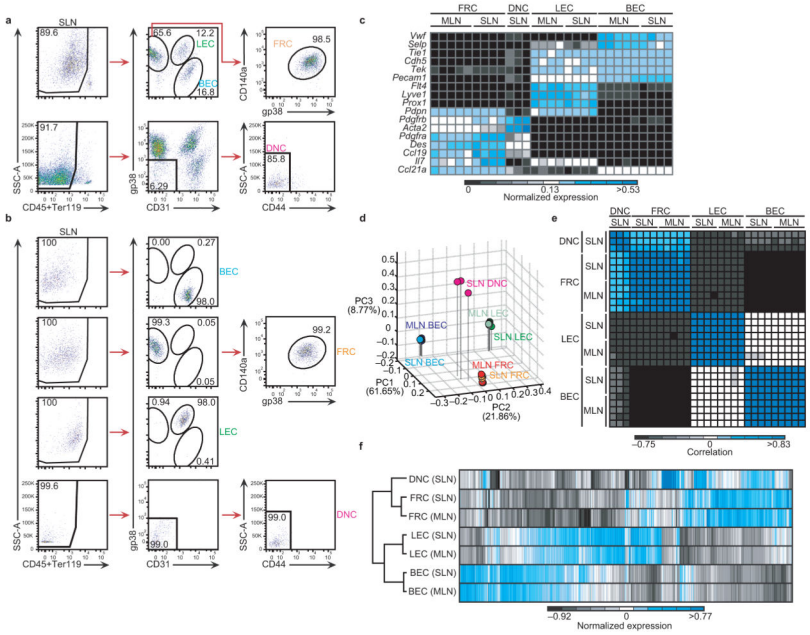

Figure 1.

Lymph node stromal cell sorting strategy and validation. **(a)** Sorting strategy used to isolate FRCs, LECs, BECs, and DNCs from stromal-cell enriched fractions of pooled SLNs or MLNs. Percentages of CD45$^-$ stroma (left) and each LNSC subset (center and right) are shown. Data represent 3-5 experiments. **(b)** A representative post sort purity analysis of SLN FRCs, LECs, BECs, and DNCs. Data shown are representative of 3-5 independent replicates. **(c)** Heatmap depicting expression of genes characteristic of FRCs, LECs, or BECs. Microarray expression values were row-normalized using the "Hierarchical Clustering" module (GenePattern). **(d)** Principal component analysis of LNSC subsets calculated on the 15% most differentially expressed probes (EV>120 for any subset) among LNSC subsets. Percentages reflect the proportion of total variability explained by each principal component. Expression values were $\log_2$ transformed and standardized across rows and columns prior to computing principal components. **(e)** Heatmap representation of coefficients of correlation computed using the 15% most differentially expressed probes among LNSCs. Most highly correlated samples are shown in blue. Expression value data was $\log_2$ transformed and row-standardized. **(f)** Unbiased hierarchical clustering of differentially expressed probes (EV>120 for any population, FC>2 in any pair-wise population comparison, and CV<0.5 within each population). Population expression values (EV) were $\log_2$ transformed, row mean-centered, and row-normalized using the "Hierarchical Clustering" module (GenePattern) before clustering. Population means were computed from 3-5 independent replicates.

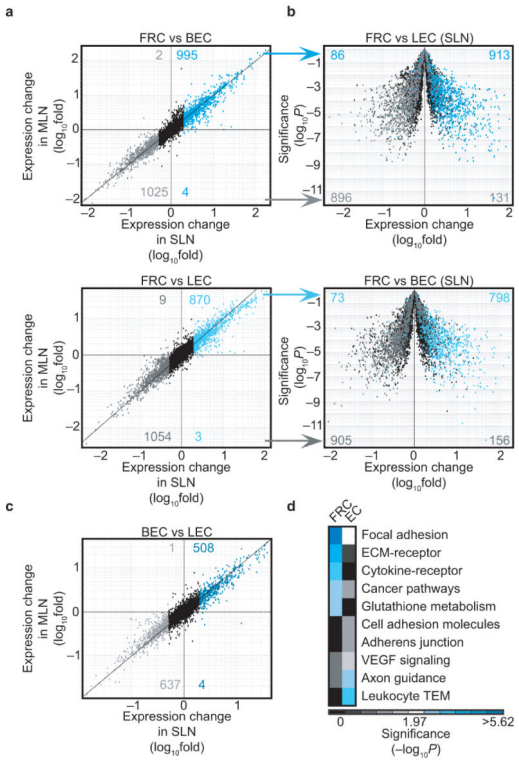

Figure 2.

Unbiased analysis of lymph node stromal cells provides insight into FRC function. **(a)** Fold change (FC)-FC comparisons of FRC expression profiles with BEC (top) or LEC (bottom) profiles. SLN and MLN data are displayed. Probes falling along the diagonal show similar expression in both sites. Probes upregulated (FC>2, EV>120 for at least one LNSC subset, and CV<0.5 for all LNSCs) in SLN FRCs are blue. Probes upregulated by SLN BECs (top) or SLN LECs (bottom) are gray. Numbers of probes in each quadrant are labeled. Data consist of 4-5 independent replicates. **(b)** Probes identified in (a) were projected onto volcano plots (fold change versus *P* value) of SLN FRCs and the other SLN endothelial subset (top: LECs, bottom: BECs). Numbers denote total highlighted probes on that side of the y-axis. Data consist of 4-5 independent replicates. **(c)** FC-FC analysis of BEC and LEC expression profiles. Upregulated probes (FC>2, EV>120 for at least one LNSC subset, and CV<0.5 for all LNSCs) in BECs (blue) or LECs (gray) are highlighted. Data consist of 4-5 independent replicates. **(d)** Enrichment in KEGG pathways for probes upregulated (δ=1.0 (adjusted FC≥2) for at least one comparison and δ=0.85 (adjusted FC≥1.8) for all other comparisons; P<0.05 for differences in expression) in FRCs relative to ECs or vice versa. Most significantly enriched (Benjamini *P* value) pathways (mmu04510:focal adhesion, mmu04512:ECM-receptor interaction, mmu04060:cytokine-cytokine receptor interaction, mmu05200:pathways in cancer, mmu00480:glutathione metabolism, mmu04514:cell adhesion molecules, mmu04520:adherens junction, mmu04370:VEGF signaling pathway, mmu04360:axon guidance, and mmu04670:leukocyte transendothelial migration) are shown in blue.

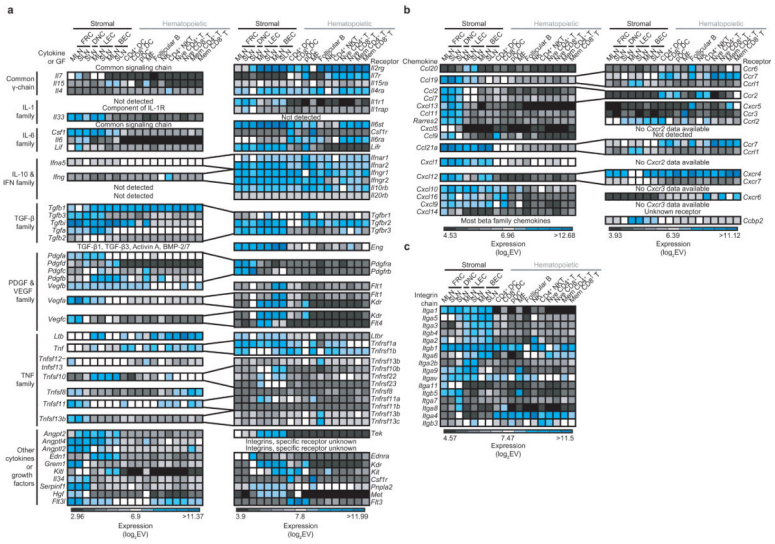

Figure 3.

Expression of cytokines, growth factors, and immunologically relevant receptors by stromal and hematopoietic cell subsets. **(a)** Heatmap analysis of cytokine, growth factor, and receptor expression (EV>120 for the receptor or ligand in any stromal population) among LNSCs and 11 LN hematopoietic subsets. Data was $\log_2$ transformed. Data represent 3-5 independent replicates. **(b)** Chemokine and chemokine receptor analysis as in (a). **(c)** Integrin expression analysis as in (a).

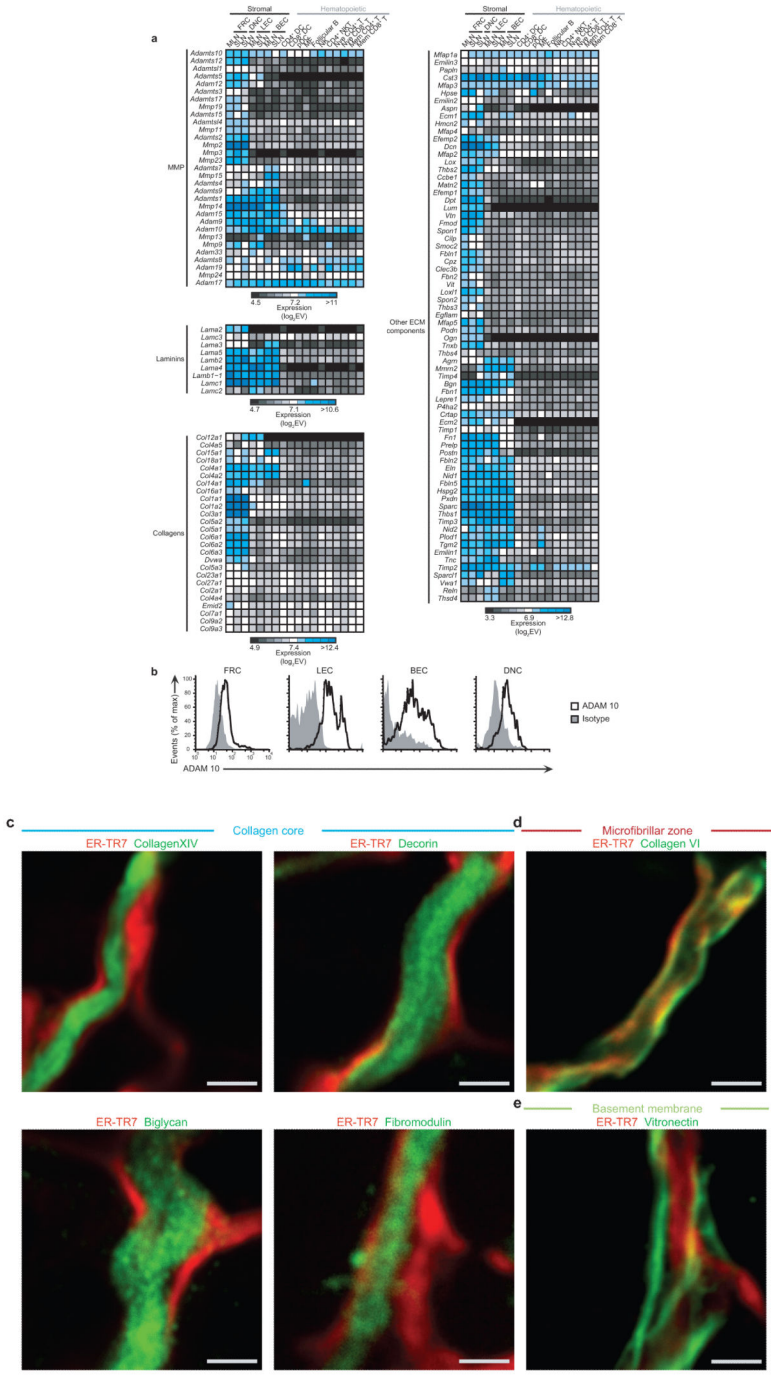

Figure 4.

Transcriptional insights into the lymph node conduit network. **(a)** Proteinaceous ECM components were identified by gene ontology (AmiGO). Representative heatmaps of expressed probes (EV>120 for any LNSC population) are shown. Data has been $\log_2$ transformed; more highly expressed probes are shown in blue. Data represent 3-5 independent replicates. **(b)** Flow cytometric analysis of ADAM 10 (unshaded, black) expression by freshly isolated SLN FRCs, LECs, BECs, and DNCs relative to an isotype

control (shaded, gray). Data represent n=7 mice from 3 independent experiments. **(c)** High magnification confocal immunofluorescent images of T-zone reticular fibers costained for the ER-TR7 antigen (red) and novel collagen core components (green): collagen XIV (top left), decorin (top right), biglycan (bottom left), and fibromodulin (bottom right). **(d)** Costaining of ER-TR7 (red) and the novel microfibrillar zone constituent, collagen VI (green) as in (c). **(e)** Costaining of ER-TR7 (red) and the newly localized basement membrane component: vitronectin (green) as in (c). Scale bars are 2 μm for all images. Data represent 4-5 independent experiments.

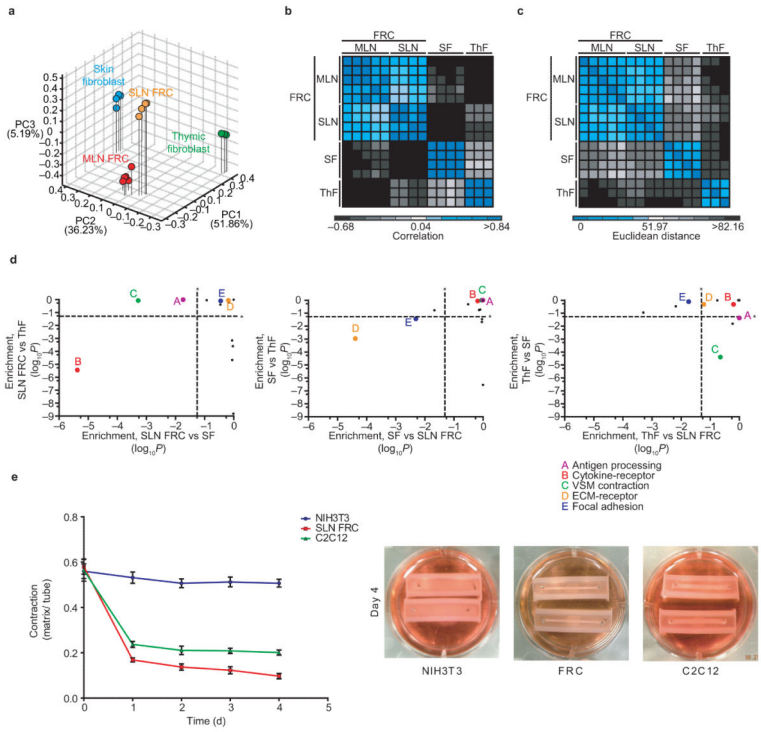

Figure 5.

Transcriptional specialization of fibroblastic reticular cells, thymic fibroblasts, and skin fibroblasts. **(a)** Principal component analysis of the 15% most differentially expressed probes among SLN FRCs, MLN FRCs, skin fibroblasts (SFs), and thymic fibroblasts (ThFs). Expression values were $\log_2$ transformed and standardized across rows and columns before calculating principal components. **(b)** Heatmap of Pearson coefficient of correlation values computed using the 15% most differentially expressed probes identified in (a). Samples with highest correlation are shown in blue. Expression data was $\log_2$ transformed and row-standardized prior to analysis. **(c)** Heatmap of Euclidean distances calculated on the 15% most differentially expressed probes identified in (a). Data was transformed as in (b). Samples with the smallest distance are shown in blue. **(d)** Significant (Benjamini $P<0.05$) hits from pooled KEGG pathway enrichment analyses of cell type-specific lists generated from pairwise "Delta Score" and "Multiplot" analyses (GenePattern, $\delta=1$ (adjusted FC≥2), $P<0.05$) were plotted on scatter plots. Benjamini P values are shown in terms of FRC enrichment (left), SF enrichment (middle), or ThF enrichment (right). 5 biologically interesting hits (mmu04612:antigen processing and presentation, mmu04060:cytokine-cytokine receptor interaction, mmu04270:vascular smooth muscle contraction, mmu04512:ECM-receptor interaction, and mmu04510:focal adhesion) are shown in color. **(e)** Contractile activity of FRCs, NIH3T3 fibroblasts, and C2C12 myoblasts was compared *in vitro*. Data are representative of 2 experiments. Data are shown as mean±SD. $*P < 0.05$.

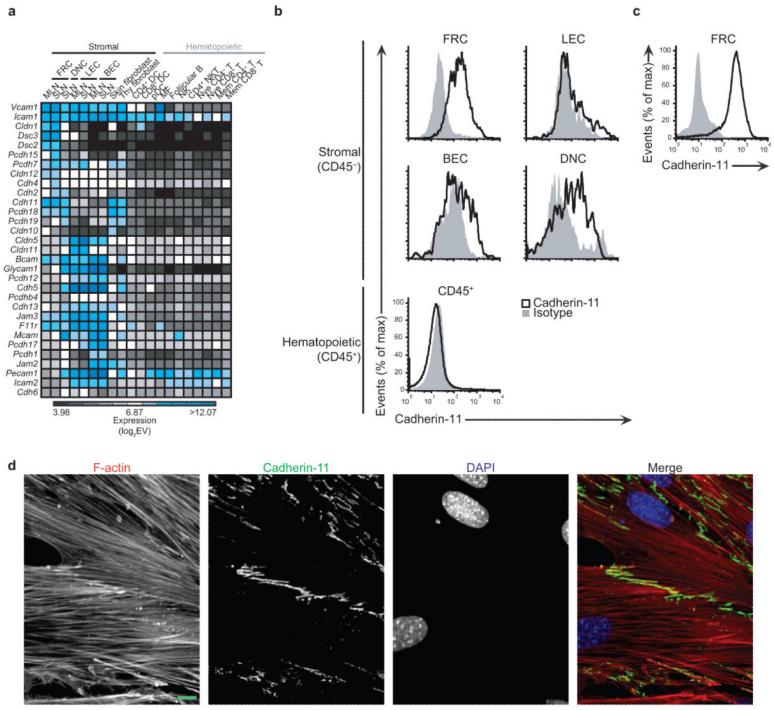

Figure 6.

Cadherin-11 identifies junctions between lymph node fibroblastic reticular cells. **(a)** Stromal and hematopoietic cell expression value data for candidate cell adhesion molecules. Expression values were $\log_2$ transformed. Data represent 3-5 independent replicates. **(b)** Flow cytometric analysis of cadherin-11 expression (unshaded, black) compared to a relevant isotype control (shaded, gray) in freshly isolated FRCs, LECs, BECs, DNCs, and bulk hematopoietic cells. Data represent 4 independent experiments. **(c)** Surface expression of cadherin-11 on *in vitro* expanded FRCs as in (b). Data represent 4 independent experiments. **(d)** Confocal immunofluorescence analysis of cadherin-11 (green) localization on *in vitro* expanded FRCs (f-actin, red; DAPI, blue). Scale bar is 10 μm. Images are representative of 4 independent experiments.

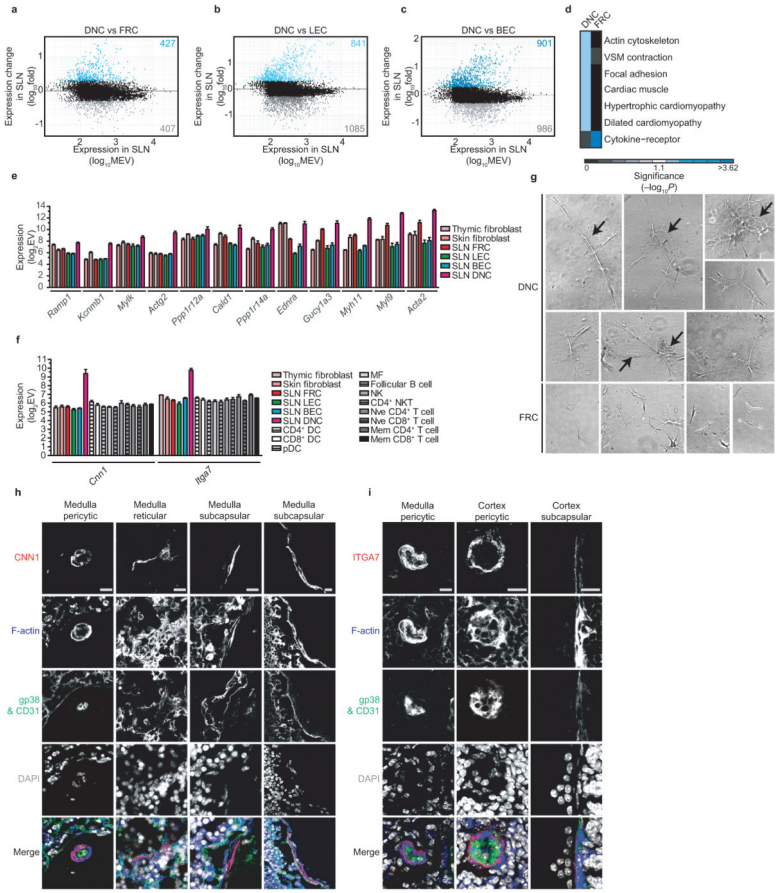

Figure 7.

DNCs are contractile pericytes. **(a)** 2-class-EV versus FC plot of SLN DNCs and FRCs. Upregulated probes (EV>120 for any LNSC subset, FC>2, CV<0.5) are highlighted in blue (DNCs) or gray (FRCs). Numbers of upregulated probes are indicated. Data represent 3-4 independent replicates. Analysis of SLN DNCs and LECs **(b)** or BECs **(c)** as in (a). Data represent 3-4 independent replicates. **(d)** KEGG pathway enrichment by probes upregulated (δ=1 (adjusted FC≥2), P<0.05) in SLN DNCs relative to SLN FRCs or vice versa. Most significantly enriched (Benjamini *P* value) pathways (mmu04810:regulation of actin cytoskeleton, mmu04270:vascular smooth muscle contraction, mmu04510:focal adhesion, mmu04260:cardiac muscle contraction, mmu05410:hypertrophic cardiomyopathy, mmu05414:dilated cardiomyopathy, and mmu04060:cytokine-cytokine receptor interaction) are shown in blue. **(e)** LNSC, SF, and ThF expression of 12 vascular smooth muscle-associated genes upregulated in DNCs relative to FRCs. Data represent 3-4 independent replicates. Data are shown as mean+SD. **(f)** Stromal and hematopoietic expression of candidate DNC markers: calponin-1 (*Cnn1*) and integrin α7 (*Itga7*). Data represent 3-4 independent replicates. Data are shown as mean+SD. **(g)** Brightfield microscopy (original magnification: 100x) showing sorted FRCs and DNCs grown in a 3D-matrigel for 5 days. Arrows indicate visible matrix contraction. Data represent 3 independent experiments. **(h)** Immunofluorescence microscopy showing expression of ITGA7, F-actin, and DAPI. Cells were confirmed as DN by excluding gp38 and CD31 staining. Scale bar is 15 μm. Data

represent 3 independent experiments. **(i)** Immunofluorescence microscopy showing expression of CNN1, F-actin, and DAPI as in (h). Scale bar represents 15 μm. Data represent 3 independent experiments.

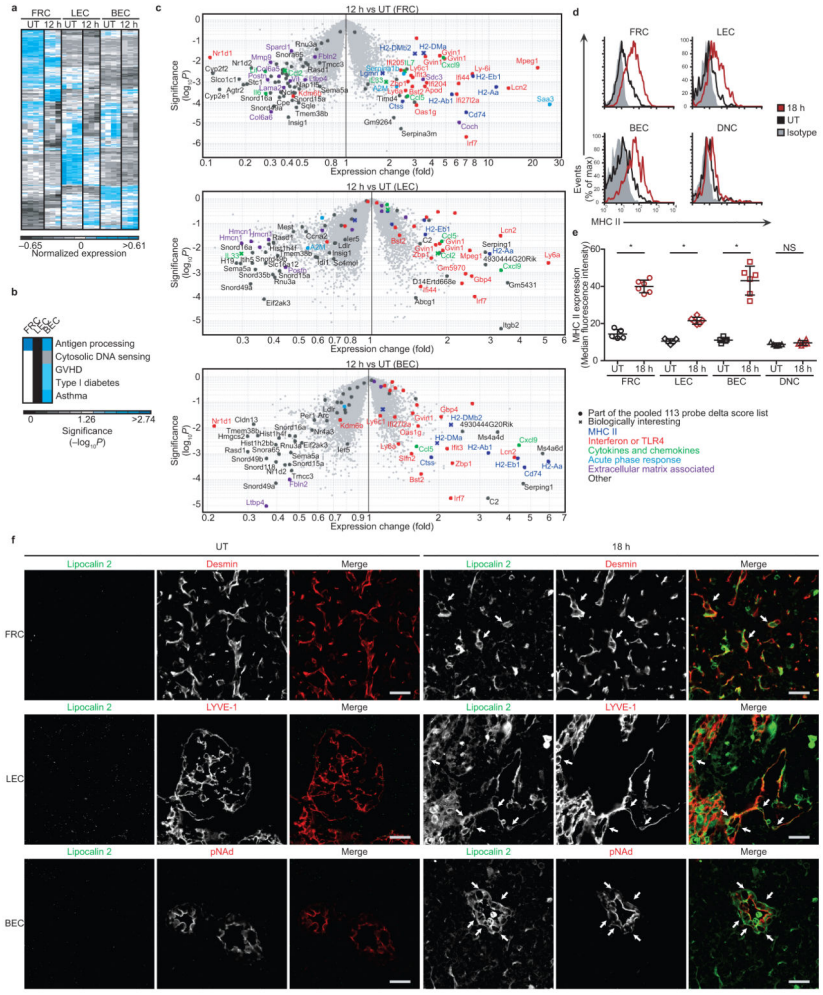

Figure 8.

LNSC response to inflammation. **(a)** Unbiased hierarchical clustering of 373 probes differentially expressed between corresponding stromal subsets from 12 h and untreated mice (EV>120 for either population, FC>2, and CV<0.5 within each population). Population EVs were $\log_2$ transformed, row mean-centered, and row-normalized using the "Hierarchical Clustering" module (GenePattern). Population means computed from 3-5 independent replicates. **(b)** KEGG pathway enrichment by probes upregulated (δ=1.0 (adjusted FC≥2), P<0.05) in 12 h LNSCs. Most significantly enriched (Benjamini P) pathways (mmu04612:antigen processing and presentation, mmu04623:cytosolic DNA-sensing pathway, mmu05332:graft-versus-host disease, mmu04940:type I diabetes mellitus, and mmu05310:asthma) shown in blue. **(c)** Projection of the 113 probes identified in (b) onto volcano plots of FRCs, LECs, and BECs from 12 h and untreated mice. Probes were biologically categorized. Data consist of 3-5 independent replicates. **(d)** Flow cytometric analysis of surface MHC II expression by SLN LNSCs from untreated (unshaded, black) and 18 h (unshaded, red) mice relative to an isotype control (shaded, gray). Data represent n=5-6 mice per condition from 2 independent experiments. **(e)** Summary median fluorescence intensity data for LNSC surface MHC II expression as in (d). Symbols

represent individual mice; mean±SD is shown. Data represent n=5-6 mice per condition from 2 independent experiments. **(f)** Confocal immunofluorescence microscopy of SLN sections costained for LCN2 (green) and desmin (red, FRCs), LYVE-1 (red, LECs), or pNAd (red, BECs) from untreated and 18 h mice. Scale bar is 25 μm. Data represent n=5-6 mice per condition from 2 independent experiments. Arrows highlight examples of LCN2-expressing stroma.